Investigation of Structural, Mechanical, Thermal and Optical Properties of Cu Doped TiO₂

Muna Muzahim Abbas, Mohammed RASHEED

Applied Sciences Department, University of Technology, Baghdad, Iraq

E-mail: munamuzahim@gmail.com

Corresponding author: rasheed.mohammed40@yahoo.com

Abstract

In this work, Pure and Cu:doped titanium dioxide nano-powder were prepared through a solid-state method. The dopant concentrations in atomic percentage were (0 - 7) wt% of samples Cu/TiO₂. Structural properties of the samples was analyzed by XRD and revealed that all nano powders of titanium dioxide having polycrystalline nature. Physical and Morphological studies were conducted using scanning electronic microscope SEM to check the grain size and texture. The other properties of samples were examined using optical microscope, Lee's Disc, Shore D hardness instrument, Fourier-transform infrared spectroscope (FTIR) and Energy-dispersive X-ray spectroscopy (EDX). Results showed that the thermal conductivity increased with the weight fraction of Cu element increasing then decreasing.

دراسة الخصائص التركيبية، الميكانيكية الحرارية والبصرية لثنائي اوكسيد التيتانيوم المشوب بالنحاس

منى مزاحم عباس، محمد رشيد

قسم العلوم التطبيقية، الجامعة التكنولوجية، بغداد، العراق

الخلاصة

في هذا البحث، تم تحضير مسحوق النحاس النانوي النقي والمشوب بثاني أكسيد بطريقة الحالة الصلبة. تم اشتقاق تركيز المشوب [نحاس/ ثنائي اوكسيد التيتانيوم في النسبة المئوية الذرية (wt٪)] من 0 إلى 7٪ بالوزن. أظهرت الخصائص التركيبية للعينات التي أجريت باستخدام XRD أن جميع المساحيق النانوية هي من ثاني أكسيد التيتانيوم ذات الطبيعة متعددة التبلور. أجريت الدراسات الفيزيائية والسطحية باستخدام المجهر الإلكتروني الماسح SEM لتأكيد حجم الحبيبات وملمسها. تم فحص الخصائص الأخرى للعينات باستخدام المجهر الضوئي، قرص لي، أداة قياس الصلابة (شور D)، مطيافية الأشعة تحت الحمراء لتحويل فورير (FTIR) والتحليل الطيفي للأشعة السينية المشتتة للطاقة (EDX). أظهرت النتائج أن الموصلية الحرارية تزداد بزيادة الكسر الوزني لعنصر النحاس ثم تقل.

Introduction

In recent years, several metal oxides such as Titanium dioxide (TiO₂), zinc oxide (ZnO), bismuth oxide (Bi₂O₃), nickel oxide (NiO), and indium oxide (In₂O₃) in both pure and doped forms have been demonstrated [1-3]. Titanium dioxide (TiO₂) has gained prominence because of its availability, non-toxicity and a cheapness compared to others .It has an indirect optical band gap up to (3.2-3.35) eV at room temperature with a high absorption coefficient. The interest on different characteristics of Cu:TiO₂

(CTO) nanomaterials is huge due to its practical importance in technology for example, photocatalytic activity [4], gas sensing [5], antimicrobial [6], antibacterial activity [7] and dye sensitized solar cell (DSSC) [8]. Cu doped TiO_2 could be doped in a large number of synthesis techniques such as solid-state method [9-11], sol-gel method [12-15], hydrothermal process [17, 18] … etc.

In this paper, A study of the structural, morphology, thermal and optical properties of pure and Cu:doped TiO_2 (CTO) nanoparticles, fabricated by solid-state method at 1100 ^{o}C, is presented The dopant concentrations of Cu were varied over the range (0 – 7) wt%.

Experimental

Commercial copper and titanium dioxide nano-sized Cu and TiO_2 nanopowders (Sigma-Aldrich Company with a high purity 99.99%) were used to synthesize the pure and mixed CTO samples. A high temperature solid state method was employed to prepare CTO pellets of Cu:TiO_2 of concentrations (3%, 5%, 7%) using high purity Cu particles and TiO_2 NPs powder. The particle size diameter was 20 nm for the pure TiO_2 NPs pure. Pure alumina crucible was utilized to mix the powders in an agate mortar for three hours and calcined at 627 K for seven hours. After cooling, the powder was re-calcined again at 727 K for seven hours. Finally, the pellets were sintered at 1373.15 K for seven hours. Pellets of 1.1 mm thickness and 8 mm diameter under pressure 5 tons were used for the different measurements. For example: X-ray diffraction (XRD) of powders for the compound was reported at ambient temperature (27 ^{o}C =-246.15 K) using (SHIMADZU-6000 2 kW type) diffractometer, with Cu, NF type (60 kV, 80 mA, $\lambda = 1.5418\,A^o$) radiation in Bragg angles ($0^o \leq \theta \leq 100^o$) at 1000°/min (scanning rate), and 185 mm (scanning radius).

In addition, Morphological study of samples was investigated with digital optical microscope (type RoHS-1600X), and scanning electron microscope (SEM), (INSPEC S50, USA). An energy dispersive X-ray spectroscope (EDX) (type INSPEC S50) was used in order to recognize the presence of constituents in the prepared samples. A Fourier Transform Infrared Spectroscope (FTIR) (using SHIMADZU model (spectrum 400)) is a good powerful instrument to calculate the bonding between the molecules in the spectral wavelength range is betwee (400 to 4000) cm^{-1}.

Moreover, Durometer Hardness (type (Shore D) (Time group INC.)) was used to measure the thoroughly hardness values of the prepared samples. Lee's Disc (Griffen and George Ltd, Britain Company) was used to obtain the thermal conductivity of prepared samples. The roughness test instrument type (Portable Roughness Tester User's manual TR220) was utilized to determine the roughness of the prepared samples.

Results and discussion

Figs. 1 and 2 deals with the physical properties of the samples. In both figures 0 refers to the pure titanium dioxide samples, while; 1 refers to the pure copper and then to the % weight of copper added to nanoscale titanium dioxide.

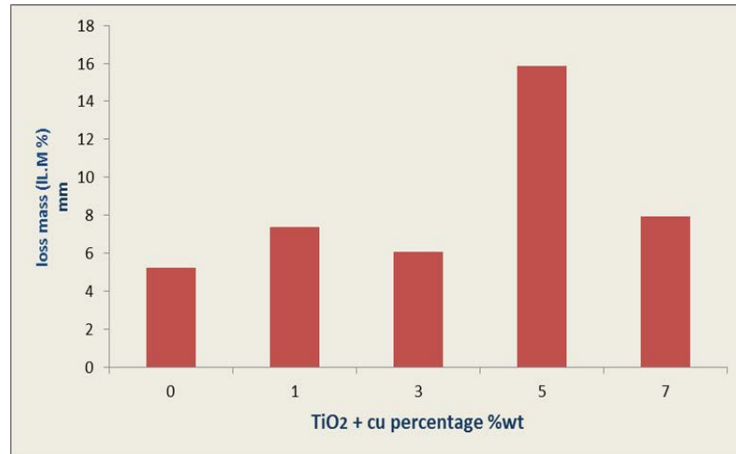Fig. 1 presents the mass change of the samples before and after calcination at 1373.15 K.

Fig. 1: Loss in mass of samples after calcination at 1373.15 K.

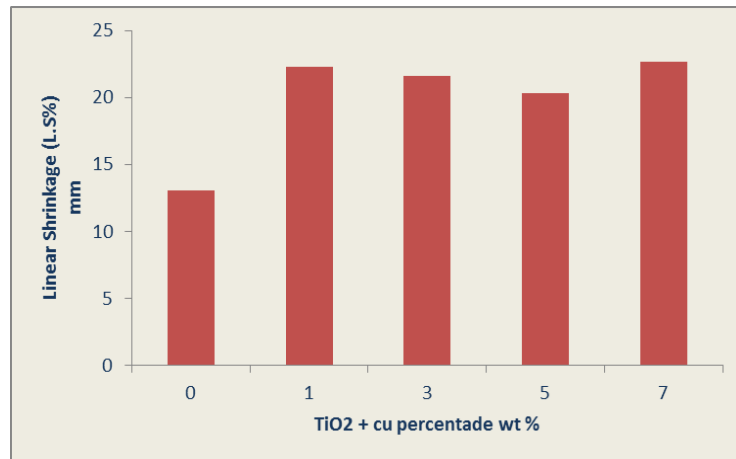Fig. 2 shows the change in length due to the addition of copper to titanium dioxide.

Fig. 2: Longitudinal shrinkage of samples after calcination at 1373.15 K.

The XRD patterns of pure TiO_2 pure and TiO_2 doped with various weights of copper (0-7) wt% (calcined at 1373.15 K) are shown in Figs. 3-6. The XRD profiles for pure titanium dioxide and CTO , achieved with (40 kV, 30 mA) operation setup, show peaks indexed to planes (110), (101), (200), (111), (210), (211), (220), (002) and (310) at 2θ data of 28.0100^o, 36.6314^o, 39.7407^o, 41.7937^o, 44.6033^o, 54.8446^o, 57.1709^o, 63.2395^o and 64.5555^o , respectively. This figure corresponds to anatase phase of TiO_2 (JCPDS Card No. 86-0148). Increase in the intensity of the peaks can be noticed as the Cu concentration increases (at annealing temperature 1373.15 K). This behavior is because of the improve of the crystallite structure with the increase of the concentration of dopant and because of the high calcination temperature. In addition, it can be seen that 2θ values after annealing have shifted towards higher values because atoms occupying the sites inside the crystal structure changes the data of (d_{hkl}).
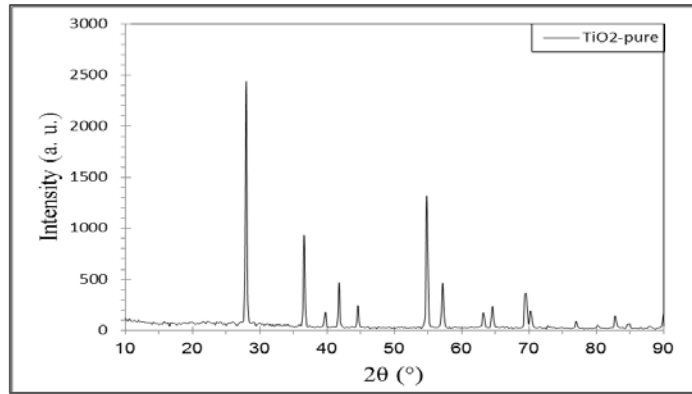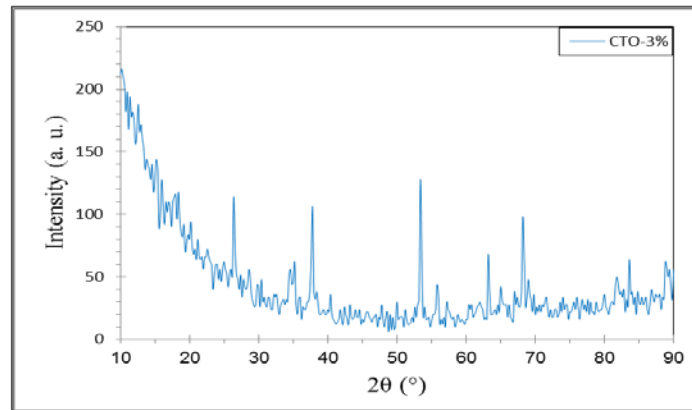
3

Fig.3: XRD curves of TiO₂ pellet.

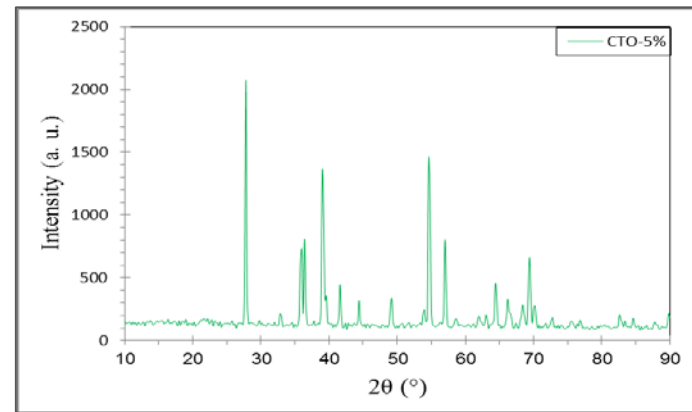*Fig. 4: XRD curves of CTO pellet with 3% wt Cu.*

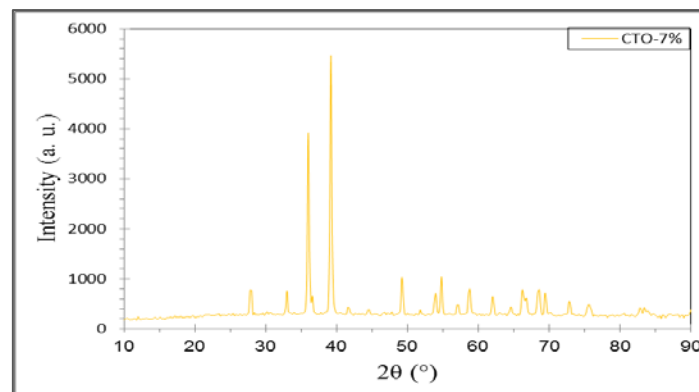*Fig.5: XRD curves of CTO- pellet with 5%wt Cu.*

Fig.6: XRD curves of CTO pellet with 7%wt Cu.

Scherrer's formula was utilized to determine the crystallite size d_{hkl} of the materials as follows:

$$d_{hkl} \times \beta \times \cos(\theta) = 0.89 \times \lambda \qquad (1)$$

where λ is the wavelength of X-ray=1.5418 A^o, θ is the angle at which the peaks position and β is the peak FWHM value. Based on X-ray diffraction results, the crystallite size of the TiO_2 NPs was about (20.26 to 30.84) nm.

The elemental chemical composition was identified by EDX spectra as shown in Fig. 7. The results are reported in Table 1. Ti, O, and Cu peaks have been detected.
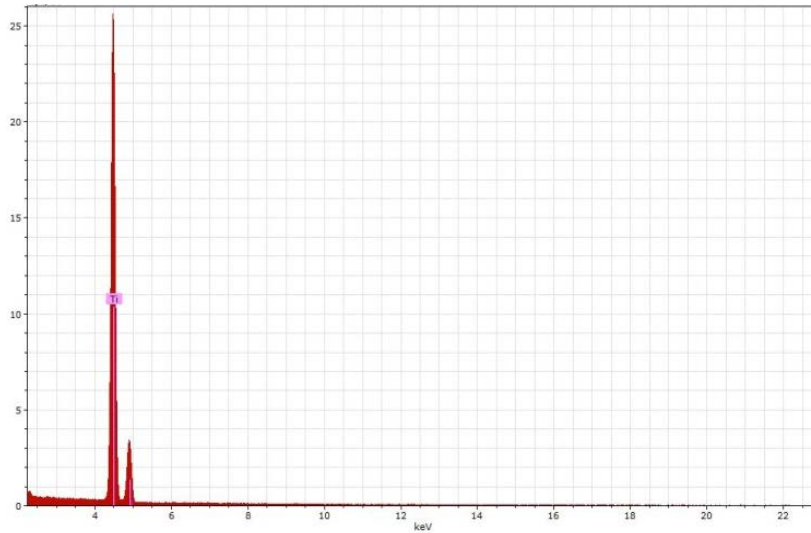

Fig. 7: EDX curves of TiO₂ NPs.

Table 1: Atomic percentage of TiO₂ nanoparticles as prepared sample corresponding to EDX test instrument.

Samples	Compositions (wt. %)				Total (%)
	Mass Ratio	O	Ti	Cu	
TiO_2	0	31.12	68.88	0	100
CTO	3%	30.58	69.04	0.38	100
CTO	7%	30.12	69.31	0.57	100
CTO	5%	28.95	70.24	0.81	100

Fig. 8 shows the micrographs images of the samples. It is clear that the best Cu concentration, for better miscibility and less homogeneity (smoother) between the TiO_2 NPs was (5% wt.) compared with the other wt % of Cu particles.
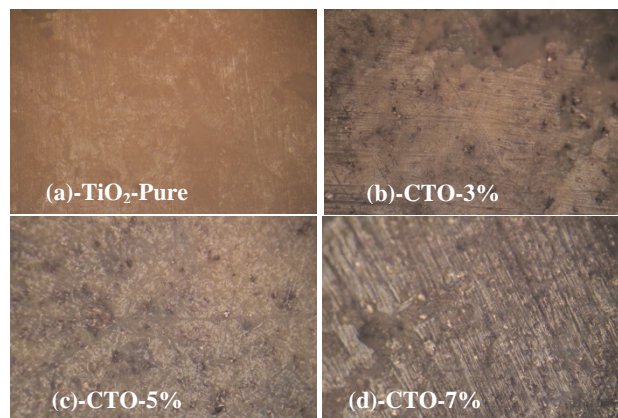

Fig. 8: Micrographs images of samples.

Fig. 9 illustrates the SEM micrographs of samples. It can be seen that the shape of particles is nearly spherical but in aggregated state. There is a decrease in the aggregations and particles size of the samples with increasing the dopant concentration (0%-7%).
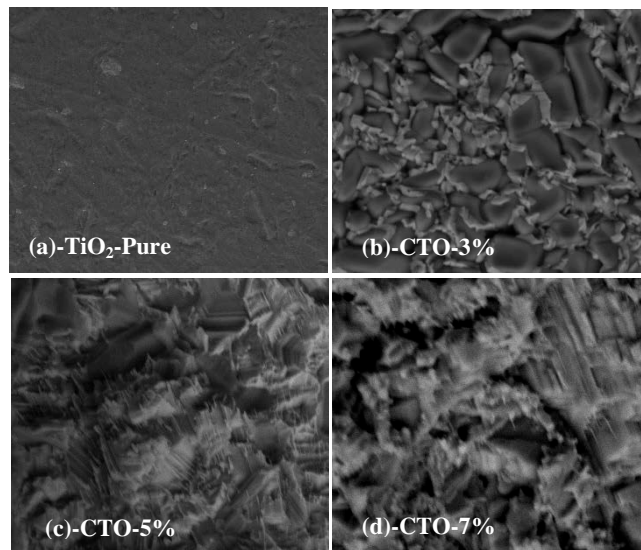

Fig. 9: SEM images of (a) 0%wt, (b) 3%wt, (c) 5%wt, and (d) 7%wt CTO NPs.

The FTIR spectra of the prepared samples in the (4000-400) cm^{-1} region are shown in Fig. 10 for all samples.
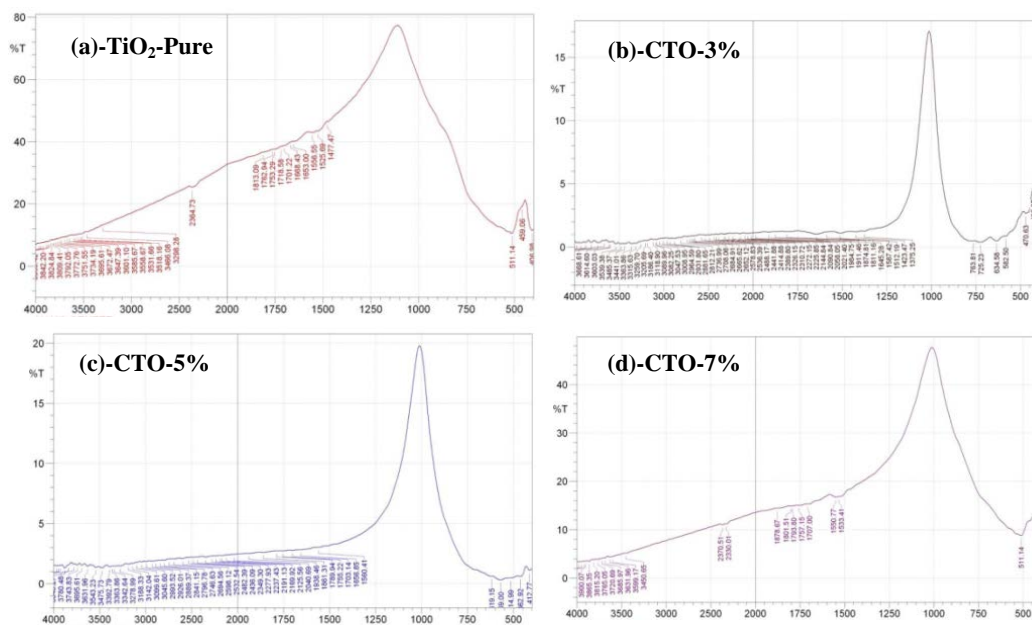

Fig. 10: FTIR spectra of samples: (a) TiO$_2$ Pure, (b) Cu:TiO$_2$-3%wt, (c) Cu:TiO$_2$-5%wt, (d) Cu:TiO$_2$-7%wt.

Table 2 gives the roughness of the prepared samples after applying pressure of 5 t (ton) to make the pellets and before and after calcination at 1373.15 K. Surface roughness is an important factor when dealing with the mechanical properties of materials such as cracks, slip, and durability. Where its effects are reflected in various applications such as: electrical, thermal resistance, fluid dynamics, and control of vibration and noise. From Table 2 it can be noticed that the value of roughness of the

surface for all samples increases with the rise of temperature and decreases with the increase of Cu concentration. This may be due to the weak binding between the base material and the copper particles. Roughness of the surface is based on many parameters for example hardness, composite content, temperature, and meandering.

Table 2: Roughness values of all samples at ambient and 1373.15K temperatures.

Roughness (µm)		
Samples	**-248.15±2 K**	**1373.15 ±2 K**
TiO$_2$ Pure	0.503	0.632
Cu Pure	0.5813	0.6725
CTO-3%	0.4542	0.5271
CTO-5%	0.4134	0.5282
CTO-7%	0.3835	0.4638

Hardness is a property that expresses the state of the surface of the material. Table 3 presents the hardness values of the samples before and after calcination at 1373.15 K. It can be seen that the hardness of the samples increases with the increase of temperature. The advantages of this measurement are to obtain high purity of the raw material and great consistency of grains.

Table 3: Hardness data of samples at ambient and 1373.15 K temperatures.

Hardness (MPa)		
Samples	**-248.15±2 K**	**1373.15 ±2 K**
TiO$_2$ Pure	60.45	63.33
Cu Pure	59.23	60.22
CTO-3%	52.45	58.36
CTO-5%	53.84	60.01
CTO-7%	58.44	62.54

Fig. 11 presents the changes of the compression strength (C.S.) of the samples with the change of the concentration of Cu, as measured by Brazilian test .C.S. is a measure of the ability of a material to withstand a compressive force applied to it. The Brazilian test is a simple indirect test method.
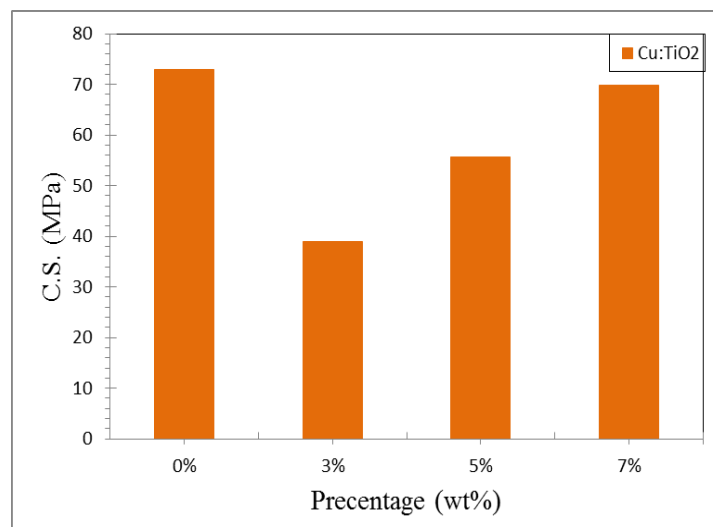

Fig. 11: Brazilian test of samples after calcination at 1373.15 K.

Thermal conductivity values of the samples were measured using Lee's disc under steady state conditions as shown in Table 4 and Fig.12.

Table 4 exhibits the effect of Cu concentration on the thermal conductivity of TiO_2 NPs. This tool consists of three discs' synthesis from brass (A, B and C) with heater connected to an electrical circuit. Heat transfers from the heater to the next two discs; after that to the third disc through the sample. T_A, T_B and T_C the temperatures of brass discs are calculated using a thermometer installed on top of the sample. The A voltage (V) of 6 V was applied to the heater while the current (I) was 0.25 A, then, the temperatures of the discs were recorded when the system approached to a steady state condition. Thermal conductivity values were determined using the following expressions:

$$H = I \times V = \pi \times r^2 e(T_A + T_B) + 2\pi re[d_A T_A + d_s \frac{1}{2}(T_A + T_B) + d_B T_B + d_C T_C] \quad (2)$$

$$KK\left(\frac{T_B - A}{d_s}\right) = e[T_A + \frac{2}{r}\left(d_A + \frac{1}{4}d_s\right)T_A + \frac{1}{2rd_s}d_s T_B] \quad (3)$$

where: H: The average time of the thermal energy generated in the coil, r: radius of the disc, T_A: temperature of disc A, T_B: temperature of disc B and T_C: temperature of disc C, d_A, d_B and d_C are the thickness of the discs A, B and C respectively, and equals to 12.5 mm, d_s: thickness of the sample under test, V: supplied voltage, I: current which pass through circuit, r: radius of the disc, e: the amount of heat transferring through cross sectional area of the sample per unit time ($\frac{W}{m^2.K}$), and K: thermal conductivity coefficient ($\frac{W}{m.K}$).

It can be seen from Table 4 that the thermal conductivity of the prepared samples increased with the increase in the ratio of Cu concentration. This is attributed to the decrease in the interfacial thermal resistance of the composite materials.

Table 4: Thermal conductivity values of all samples after calcination at 1373.15 K temperature.

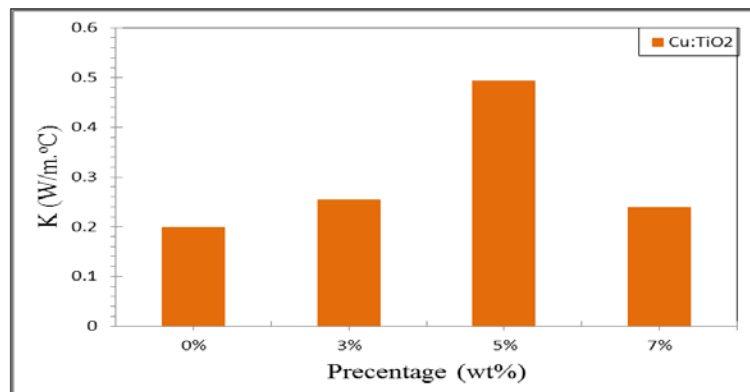| Sample	T_A°C	T_B°C	T_C°C	d_s (m)	e (W/m².°C)	K (W/m.°C)
TiO_2-Pure	30	33	33	1.30	6.551291	0.198992
Cu-Pure	28	31	31	1.76	6.788523	0.265562
3%	33	29	29	1.90	6.814051	0.254703
5%	31	33	33	1.88	6.288597	0.492845
7%	25	28	28	1.40	7.523112	0.238893

Fig. 12: Thermal conductivity of samples after calcination at 1373.15 K.

Conclusions

Pure and CTO NPs were fabricated by solid-state reaction technique. Pellets samples were calcined at 1373.15 K Surface morphology, size, and the elements for

fabricated pellets were investigated according to different quantities of copper to titanium dioxide (CTO). Mechanical properties of samples such as hardness, roughness, and thermal conductivity have been studied. Grain size of TiO_2 NPs was in the range of about (20-31) nm according to XRD. The highest percentage of mass loss was for CTO 5%wt. This means that it contains more water molecules. While, the shrinkage process increased with the increase percentage of copper added to TiO_2. The surface roughness values for all the samples increased with the rise of temperature while it decreased with the increase of Cu concentration. In addition, the value of hardness for TiO_2 was higher than the others samples before and after calcination at 1373.15 K. Moreover, the highest value for compressibility was in titanium dioxide, which indicates the material's ability to withstand compressive strength. Finally, the value of thermal conductivity for CTO 5% after calcination at 1373.15 K was the highest among the other samples.

Acknowledgment

References

[1] M. Rasheed, R. Barillé, Optical and Quantum Electronics, 49, 5 (2017) 1-14.
[2] M. Rasheed, R. Barillé, Journal of Non-Crystalline Solids, 476 (2017) 1-14.
[3] M. Rasheed, R. Barillé, Journal of Alloys and Compounds, 728 (2017) 1186-1198.
[4] M. R. D. Khaki, M. S. Shafeeyan, A. A. A. Raman, W. M. A. W. Daud, Journal of Molecular Liquids, 258 (2018) 354-365.
[5] A. Farzaneh, A. Mohammadzadeh, M. D. Esrafili, O. Mermer, Ceramics International, 45, 7 (2019) 8362-8369.
[6] A. M. Alotaibi, B. A. Williamson, S. Sathasivam, A. Kafizas, M. Alqahtani, C. Sotelo-Vazquez, I. P. Parkin, ACS Applied Materials & Interfaces, 12, 13 (2020) 15348-15361.
[7] X. Zhang, Y. Yu, D. Jiang, Y. Jiao, Y. Wu, Z. Peng, Z. Dong, Ceramics International, 45, 6 (2019) 6693-6701.
[8] A. A. Qureshi, S. Javed, H. M. A. Javed, A. Akram, M. Jamshaid, A. Shaheen, Optical Materials, 109, 110267 (2020) 1-9.
[9] S. Ahadi, N. S. Moalej, S. Sheibani, Solid State Sciences, 96, 105975 (2019) 1-10.
[10] M. Ghorbanpour, A. Feizi, Journal of Water and Environmental Nanotechnology, 4, 1 (2019) 60-66.
[11] N. S. Moalej, S. Ahadi, S. Sheibani, Journal of Ultrafine Grained and Nanostructured Materials, 52, 2 (2019) 133-141.
[12] A. Shafei, S. Sheibani, Materials Research Bulletin, 110 (2019) 198-206.
[13] M.Yıldırım, Journal of Alloys and Compounds, 773 (2019) 890-904.
[14] A. Tamarani, R. Zainul, I. Dewata, In Journal of Physics: Conference Series, 1185, 1 (2019) 012020-012025.
[15] T. Raguram, K. S. Rajni, Applied Physics A, 125(5), 288 (2019) 1-11.
[16] G. Pedroza-Herrera, I. E. Medina-Ramírez, J. A. Lozano-Álvarez, S. E. Rodil, Catalysis Today, 341 (2020) 37-48.
[17] K. Wang, R. Jiang, T. Peng, X. Chen, W. Dai, X. Fu, Applied Catalysis B: Environmental, 256, 117780 (2019) 1-12.
[18] E.W. Moon, H.W. Lee, J. H. Rok, J. H. Ha, Science of the Total Environment, 141574 (2020) 1-9.